

Unlocking the Secrets of PKS 1502+106: Synergies between mm-VLBI and Single-dish Monitoring

V. Karamanavis, L. Fuhrmann, E. Angelakis, T. P. Krichbaum, I. Myserlis, J. Hodgson, B. Boccardi, I. Nestoras, J.A. Zensus, H. Ungerechts

I. Motivated by the 2008/09 γ -ray Outburst

The processes giving rise to blazar variability remain still unclear. By combining VLBI and single dish data, we shed light on the compact regions where most of the blazar activity takes place. The blazar PKS 1502+106, at $z=1.834$, has exhibited extreme and correlated, radio and high-energy activity that triggered intense single-dish and VLBI monitoring down to 3 mm wavelength (Fig. 1). This enabled the sharpest view to date towards this extreme object.

2. PKS 1502+106 at Extreme Angular Resolution

Using ultra-high angular resolution mm-VLBI observations at 43 and 86GHz, complemented by VLBI observations at 15GHz, we explore the phenomenology and physical conditions within the ultra-relativistic jet of PKS 1502+106. The VLBI observations are complemented by single-dish radio data from the F-GAMMA program at frequencies matching the VLBI monitoring (Fig. 2). PKS 1502+106 shows a compact core-jet morphology (Fig. 1) and fast superluminal motion with apparent speeds in the range 5–22 c. Doppler factors along the jet increase from ~ 7 up to ~ 50 . This gradient implies an accelerating jet and favors scenarios of magnetic driving. The viewing angle towards the source differs between the inner and outer jet, with the former at $\theta \sim 3^\circ$ and the latter at $\theta \sim 1^\circ$, after the jet bends towards the observer, beyond 1 mas. The de-projected opening angle of the ultra-fast magnetically dominated jet is found to be $(3.8 \pm 0.5)^\circ$. A single jet component (C3) can be associated with the pronounced flare both at high energies and in radio bands.

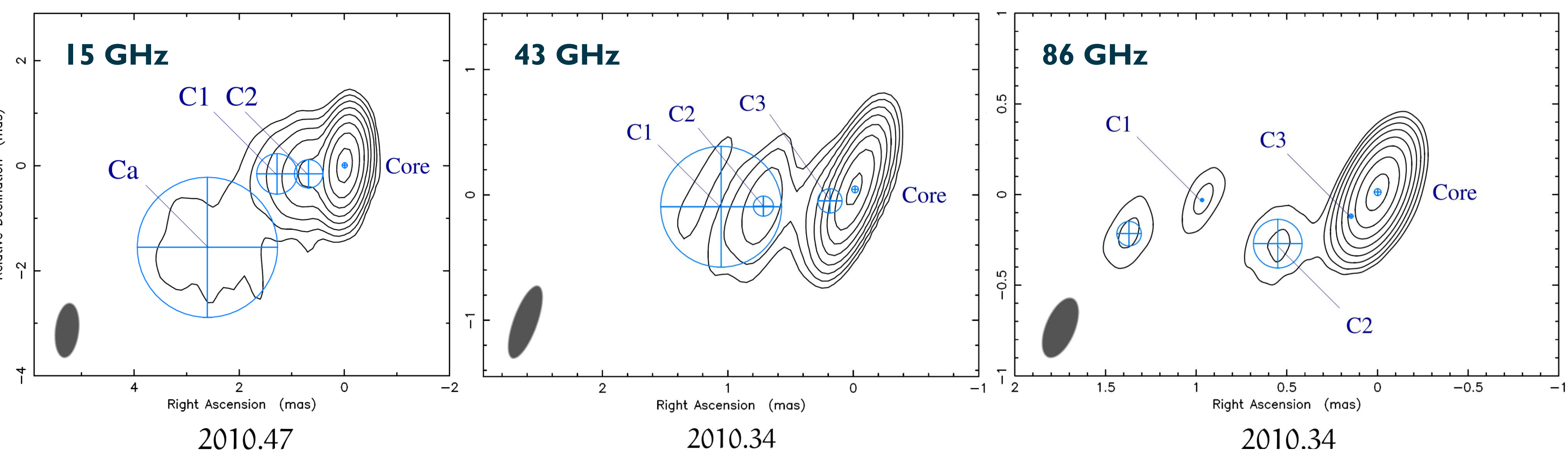


Fig. 1. Uniformly weighted MODELFIT maps of PKS 1502+106 at 15, 43, and 86 GHz. Contour levels correspond to $-0.1, 0.1, 0.2, 0.4, 0.8, 1.6, 3.2, 6.4$, and 12.8% of ~ 3 Jy/beam. A linear distance of 1 mas corresponds to about 8.5 pc. Note knot C3, responsible for the energetic outburst.

Contact: vkaraman@mpifr-bonn.mpg.de

Based on: Karamanavis 2015 [2015PhDT.....232K] //

Karamanavis et al. 2016a [2016A&A...586A..60K] // Karamanavis et al. 2016b [2016A&A...590A..48K]

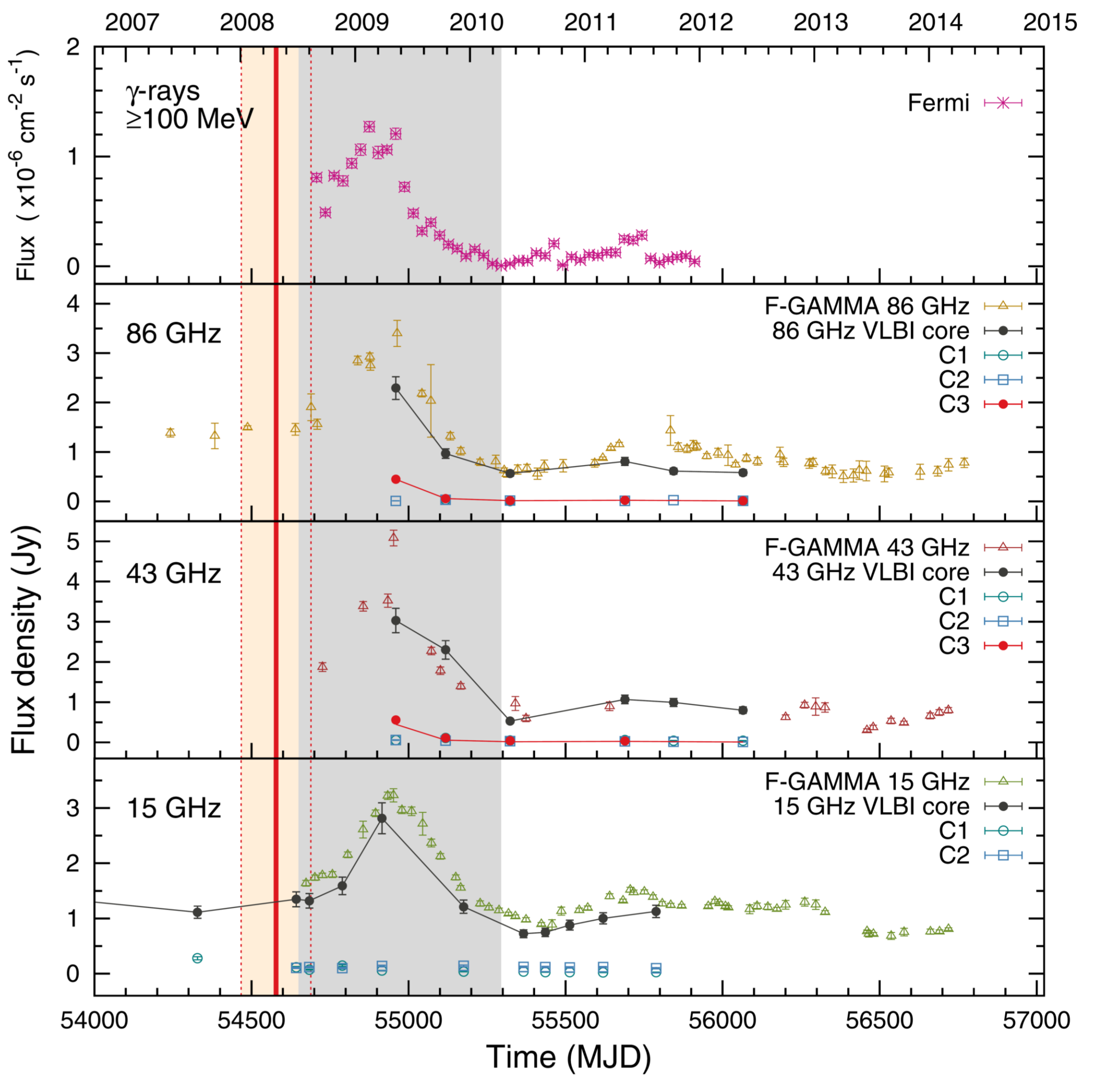


Fig. 2. Light curves of PKS 1502+106 and its VLBI knots. From top to bottom are shown the monthly binned Fermi/LAT γ -ray light curve; F-GAMMA single-dish radio light curve at 86 GHz with the core, and VLBI component light curves; same as before, but at 43 GHz and (lower panel) at 15 GHz. Knot C3 is only visible at the two highest frequencies, at its decaying flux density phase. The grey shaded area delineates the full duration of the flare ~ 650 days, while the red solid line designates the ejection time of knot C3.

3. Nuclear Opacity, Magnetic Fields and the Location of γ rays

Using the delay between the outburst maxima at different radio frequencies, we study the frequency-dependent position of core and infer its absolute position with respect to the jet base. This nuclear opacity profile enables the magnetic field tomography of the jet. We also localize the γ -ray emission region and explore the mechanism producing the flare. We do so through single-dish flux density measurements at 12 frequencies in the range 2.64 to 226.5 GHz. To quantify the outburst, we employ both a Gaussian process regression, a machine learning method (Figs. 3 and 4), and a cross-correlation function analysis. We find that the light curve parameters (flare amplitude and cross-band delays) show a power-law dependence on frequency (Fig. 5). This is consistent with a shock propagating downstream the jet. The self-absorbed radio cores are located between 10 and 4 pc from the jet base, while their magnetic fields range between 14 and 176 mG, at 2.64 up to 86.24 GHz (Table 1). Finally, the γ -ray active region is located at (1.9 ± 1.1) pc away from the jet base.

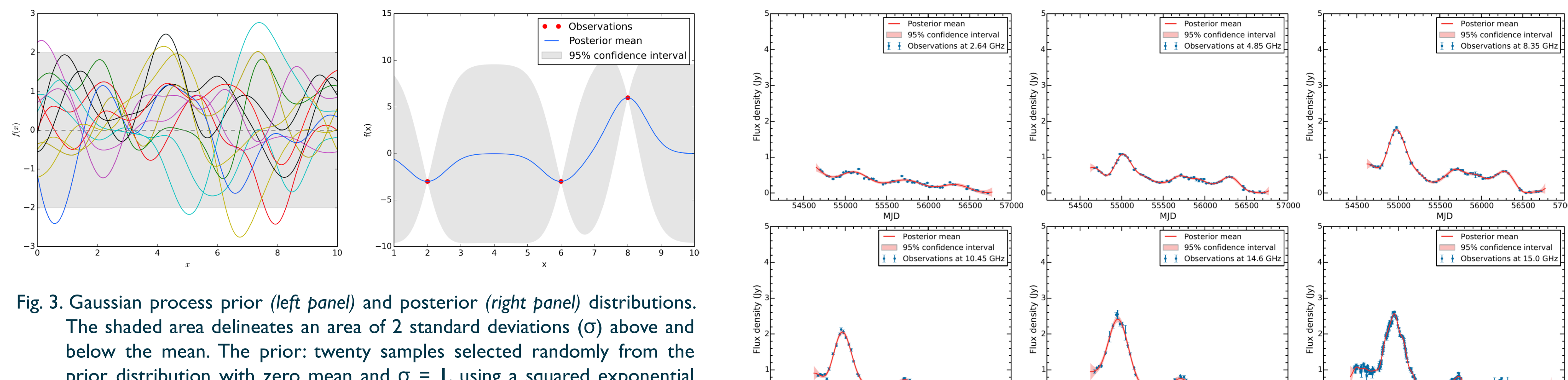


Fig. 3. Gaussian process prior (left panel) and posterior (right panel) distributions. The shaded area delineates an area of 2 standard deviations (σ) above and below the mean. The prior: twenty samples selected randomly from the prior distribution with zero mean and $\sigma = 1$, using a squared exponential kernel. The posterior: the result after training the Gaussian process with three error-free data points.

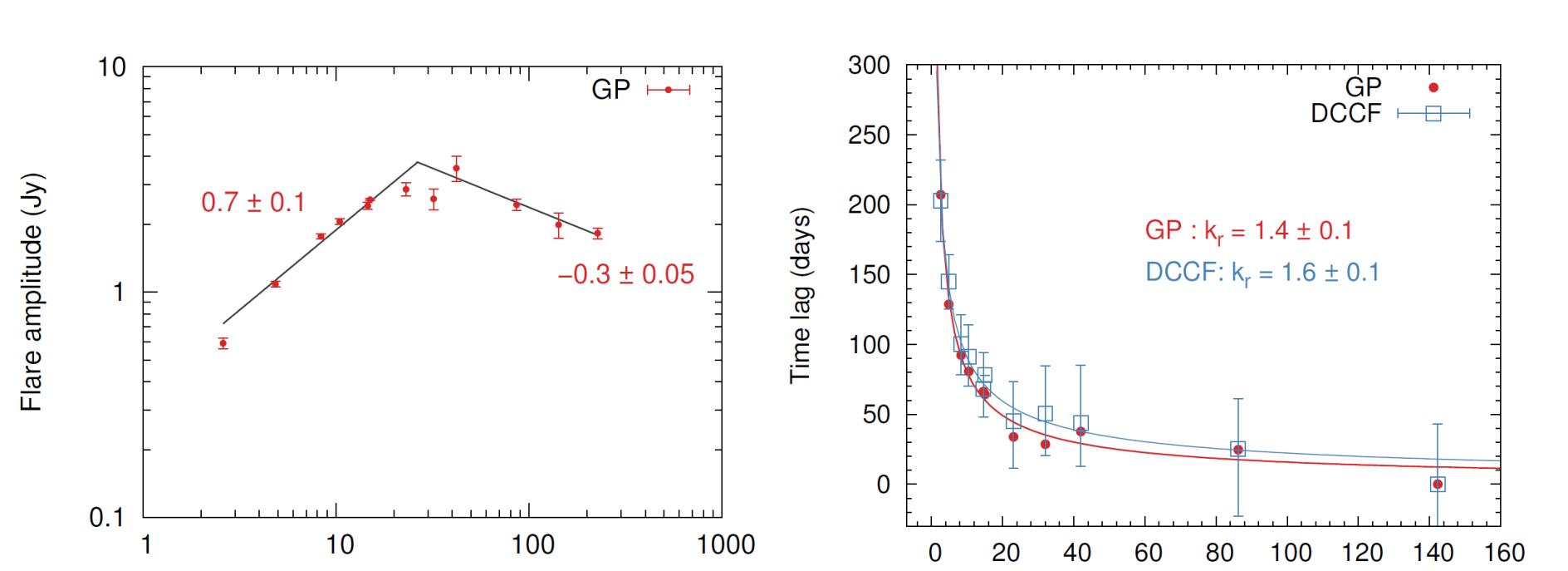


Fig. 5. Left: Frequency dependence of the flare amplitudes. Solid lines show the wings of the fitted broken power law, while the values denote their slopes. Right: Frequency dependence of the time lags w.r.t. the data at 142.33 GHz. Red circles denote values resulting from the GP regression and blue squares those from the discrete cross-correlation analysis. Solid lines represent the best fit power laws.

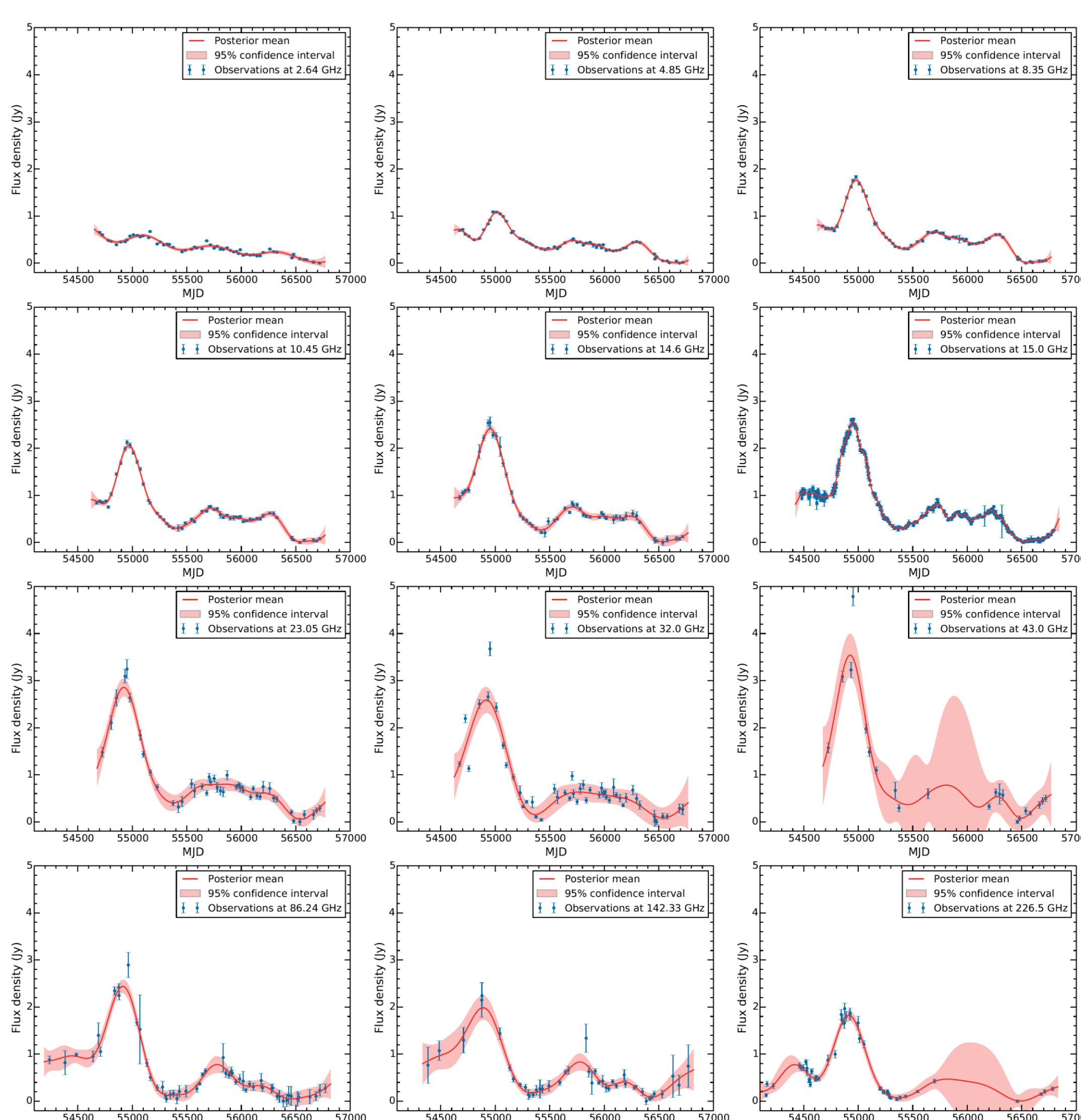


Fig. 4. Gaussian process regression curves for the radio light curves in the range 2.6–226.5 GHz. Observations are shown in blue, the posterior mean (prediction curve) in red, and the 95% confidence interval is the lighter red-shaded area.

Conclusions

1. mm-VLBI suggest an accelerating jet that bends towards us.
2. Based on the cross-band time lags, we obtain a nuclear opacity profile and a magnetic field tomography of the jet (Table 1).
3. The flare is induced by a shock seen as knot C3 in VLBI maps.
4. The γ -ray emission originates (1.9 ± 1.1) pc away from the jet base, well beyond the bulk of the BLR material.
5. This yields a contribution of IR torus photons and/or SSC to the production of γ rays, while almost negates the contribution of accretion disk or BLR photons alone.

v (GHz)	T (days)	r_{core} (pc)	B_{Ipc} [min, max] (mG)	B_{core} [min, max] (mG)
2.64	205 ± 2	10.2 ± 1.2	148 [106, 209]	14 [11, 20]
4.85	137 ± 8	7.1 ± 1.0	154 [111, 220]	22 [16, 30]
8.35	96 ± 4	5.3 ± 0.8	166 [121, 233]	32 [24, 43]
10.45	86 ± 5	4.8 ± 0.8	178 [129, 253]	37 [27, 51]
14.60	67 ± 1	4.0 ± 0.7	185 [137, 249]	46 [35, 63]
15.00	64 ± 1	3.8 ± 0.7	178 [132, 249]	47 [36, 64]
23.05	39 ± 6	2.6 ± 0.6	161 [113, 237]	62 [45, 88]
32.00	40 ± 11	2.9 ± 1.0	235 [142, 398]	80 [51, 131]
43.05	41 ± 3	3.4 ± 0.8	352 [249, 522]	102 [76, 145]
86.24	25 ± 1	4.0 ± 1.1	711 [494, 1086]	176 [129, 254]

Table 1. Synchrotron opacity structure and magnetic field tomography of the jet. Columns: (1) frequency, (2) time lag w.r.t. 142.33 GHz, (3) distance of the radio core to the jet base, (4) magnetic field strength at a distance of 1 pc from the base, and (5) core magnetic field strength.

